Pokhara Engineering College Journal (PECJ)

Applied Sciences and Engineering Insights

ISSN: 3021-9795 (Print) / 3059-9628 (Online)
(Volume-3, Issue- I)

Synthetic Inertia Emulation And Frequency Control In Distributed PV Grid Using Battery Energy Storage System

Anisha Tiwari[1*], Ajita Acharya[1], Ananta Adhikari[1]

[1]School of Engineering, Faculty of Science and Technology, Pokhara University Kaski, Nepal

**Corresponding email: tiwarianisha83@gmail.com*

Received:01- February-2026; Revised: 28- February-2026; Accepted: 25- March-2026
DOI: : https://doi.org/10.3126/pecj.v3i1.93539

Abstract

The rapid integration of distributed photovoltaic (PV) systems provides a promising solution to environmental concerns and climate obligations, yet it introduces significant challenges to power system stability. As PV penetration increases, system inertia decreases, making the grid more vulnerable to frequency deviations during contingencies such as sudden load changes, generator outages, or high PV output. Battery Energy Storage Systems (BESS) offer a viable solution by emulating synthetic inertia and providing fast frequency regulation. This study investigates the dynamic behaviour of BESS under low-inertia conditions and evaluates strategies for inertia emulation, droop-based frequency response, primary frequency response, and primary frequency regulation. An innovative approach is presented in which BESS dynamically injects or absorbs active power to mimic the inertial response of conventional synchronous generators, thereby stabilizing frequency fluctuations. The effects of BESS sizing, placement, and parameters on system performance and power losses are analyzed mathematically and through simulations. The IEEE 9-bus test system is employed to model varying PV penetration levels of 20%, 40% and 60%, along with generator outages and load scenarios. Results indicate that increasing PV penetration leads to higher Rate of Change of Frequency, deeper frequency nadir, and slower recovery. With the implementation of a 35 MVA BESS, frequency response, and steady-state frequency deviations were maintained within Nepal's operational limits of ±5% of nominal frequency. These findings demonstrate the effectiveness of BESS-based synthetic inertia in enhancing frequency stability and improving grid resilience in low-inertia, high-renewable power systems.

Keywords: Battery Energy Storage System, Synthetic Inertia, Frequency Stability, Photovoltaic Integration, Low-Inertia Power Systems, Rate-Of-Change-Of-Frequency.

1. Introduction

The worldwide energy sector is experiencing a significant shift as growing environmental concerns and climate targets are pushing the transition towards more sustainable alternatives. Clean power surpassed 40% of global electricity generation in 2024, driven by record growth in renewables (Wiatros-Motyka *et al.*, 2024). Global electricity generation grew by over 1200 TWh in 2024. Mirroring the rise in electricity demand, this annual increase of 4% represents a significant acceleration from average growth rate of 2.6% seen between 2010 and 2030. In

2024, renewables alone made up almost three-quarters of the overall increase in power generation. Solar led the way, increasing by about 480 TWh - the highest source of any and far exceeding the previous year. With this growth, installed solar PV capacity worldwide reached an estimated 2.2 TW (International Energy Agency, 2025).

Among renewable energy technologies, Photovoltaic generation is one of the fastest-growing energy sources. However, PV systems interfaced with the grid lack rotational inertia. The absence of inertial energy increases the Rate of Change of Frequency immediately following a disturbance. High RoCoF can trigger UFLS or even system collapse if not addressed. In low-inertia systems with high PV penetration, the absence of significant rotating masses results in steeper frequency drops, deeper frequency nadirs, and delayed post-disturbance recovery.

Beyond large-scale utility PV plants, distributed photovoltaic systems are increasingly contributing to total generation, particularly in urban and semi-urban areas. While DPV provides benefits such as reduced transmission losses and improved local energy autonomy, its decentralized nature further aggravates the low-inertia conditions in high PV penetration systems. Most DPV systems are interfaced through grid-following inverters, which rely on external voltage and frequency references and do not provide inherent inertial responses. As a result, widespread DPV deployment amplifies the frequency stability challenges, reducing effective system inertia and weakening the grid's natural frequency response.

To address these low-inertia challenges, Energy Storage Systems have become a vital asset for frequency regulation and grid support. Although technologies such as Pumped Hydro Storage, Flywheels, and Compressed Air Energy Storage exist as viable solutions to the grid instability issue. Battery Energy Storage Systems have emerged as one of the most effective options. Energy Storage System (ESS) have been widely proposed to compensate for the reduction in system inertia and damping caused by the displacement of conventional synchronous generators as they can emulate the dynamic behaviour of synchronous machines and provide fast acting support through function such as Inertial Response (IR) and Primary Frequency Reserve (PFR). ESS also helps reduce peak power demand by storing energy during low-demand periods and supplying it during peak hours thereby improving overall system efficiency and reliability (Amin *et al.*, 2021).

Battery Energy Storage Systems store electrical energy electrochemically in cells which are arranged in series and/or parallel to meet power and voltage requirements. Among various chemical battery such as Lead-Acid, Sodium-Sulphur, Nickel-Cadmium, and Vanadium Redox Flow, Lithium-ion stands out for its high energy density, rapid response capabilities, and comparatively longer lifespan as (Assery, Zhang and Chen, 2024).

Battery energy storage systems also offer a wide range of applications in power systems, including frequency control, voltage support, power balancing, and energy shifting. Among these, frequency control is one of the most attractive applications for grid-connected BESS, as it enables rapid restoration of system frequency following disturbances through the controlled injection or absorption of frequency-dependent power. The nature of rechargeable batteries, charging for down-regulation and discharging for up-regulation with immediate response and adjustable power scale is an inherent advantage compared with other components in the power system. The frequency response without the deadband and enhanced frequency response

without the deadband and enhanced frequency response and the service stacking cases, which promote the BESS to operate at high usage frequency since it exploits the full utilization potential of the BESS (Chunyang *et al.*, 2023).

2. Methodology

2.1 Research Framework

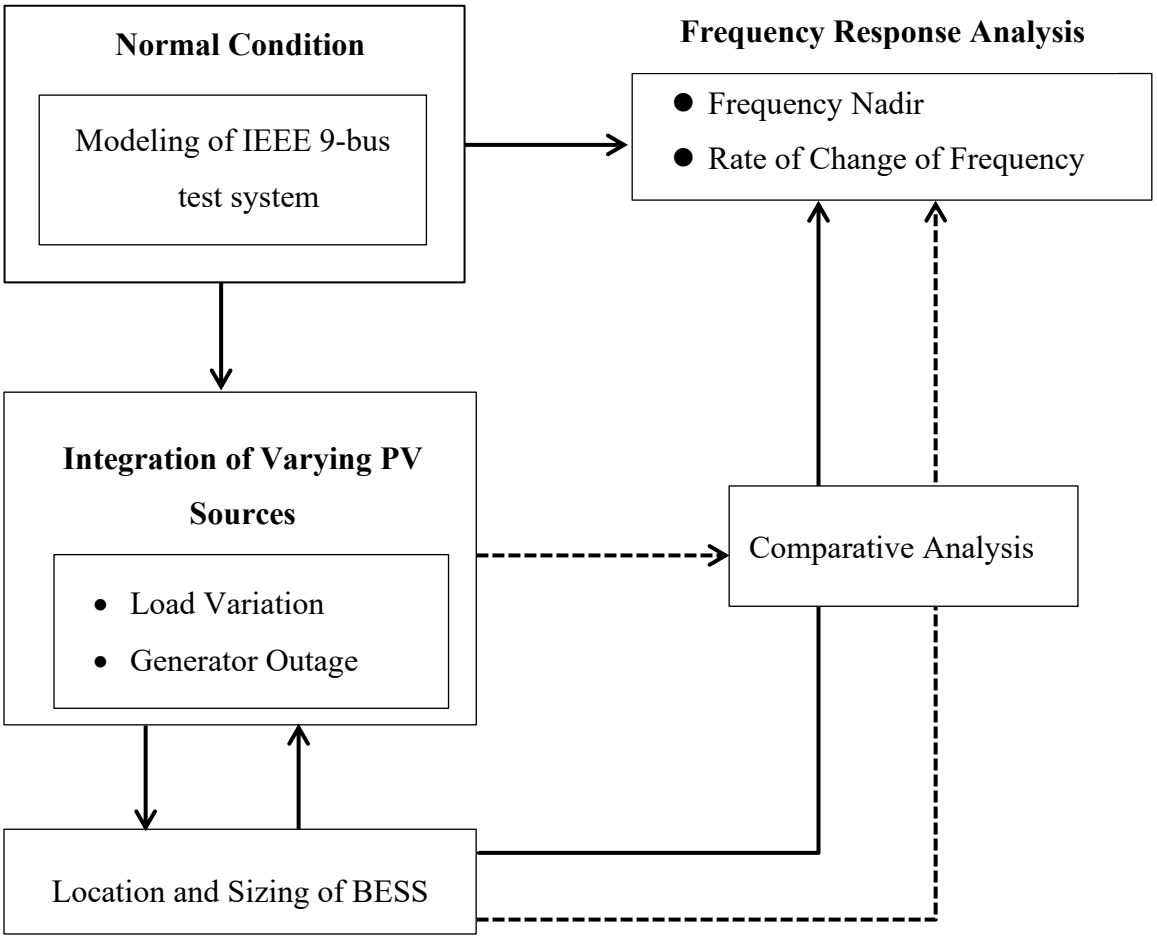

Figure 1: Block diagram of research framework

Figure 1 illustrates the research framework adopted for evaluating frequency stability in a Photovoltaic (PV)-integrated power system. Initially, the IEEE 9-bus test system is modeled under normal operating conditions. Varying levels of photovoltaic (PV) penetration are then integrated, and system disturbances such as load variations and generator outages are introduced. The frequency response is assessed using key performance indicators, including frequency nadir and Rate of Change of Frequency (RoCoF). Based on the observed dynamics, the optimal location and sizing of the battery energy Storage System (BESS) are determined. Finally, a comparative analysis is conducted to quantify the effectiveness of BESS in enhancing system frequency stability.

2.2 Power Grid Test Network

The IEEE 9-bus test system is employed as a benchmark to evaluate frequency dynamics under varying PV penetration and contingency scenarios. The network configuration and parameters are adopted from the standard IEEE 9-bus test system as detailed by P.M. Anderson (Anderson and Fouad, 2003). The system initially includes three synchronous generators, which provide

the primary source of system inertia. The transmission network is modelled using detailed line parameters, including series resistance, reactance, and line susceptance.

Each synchronous generator is equipped with detailed governor and automatic voltage regulator (AVR) models. The governor regulates turbine speed by adjusting water flow. It provides inertial support by sensing frequency deviation and modulating active power output of the synchronous generator. This rapid adjustment helps restore power balance and maintain stable system frequency (Department of Hydropower and IIT Roorkee, n.d.). An AVR maintains the generator terminal voltage at a desired level by continuously monitoring output voltage. It automatically adjusts the generator excitation current to compensate for load changes and varying operating conditions (IEEE Power System Dynamic Performance Committee, 1992).

A steady-state load flow analysis is first performed to ensure system convergence before conducting dynamic simulations. The generator, transformer and load data of the IEEE 9-bus test system is shown on Tables 1-3. The system configuration is shown in Figure 2.

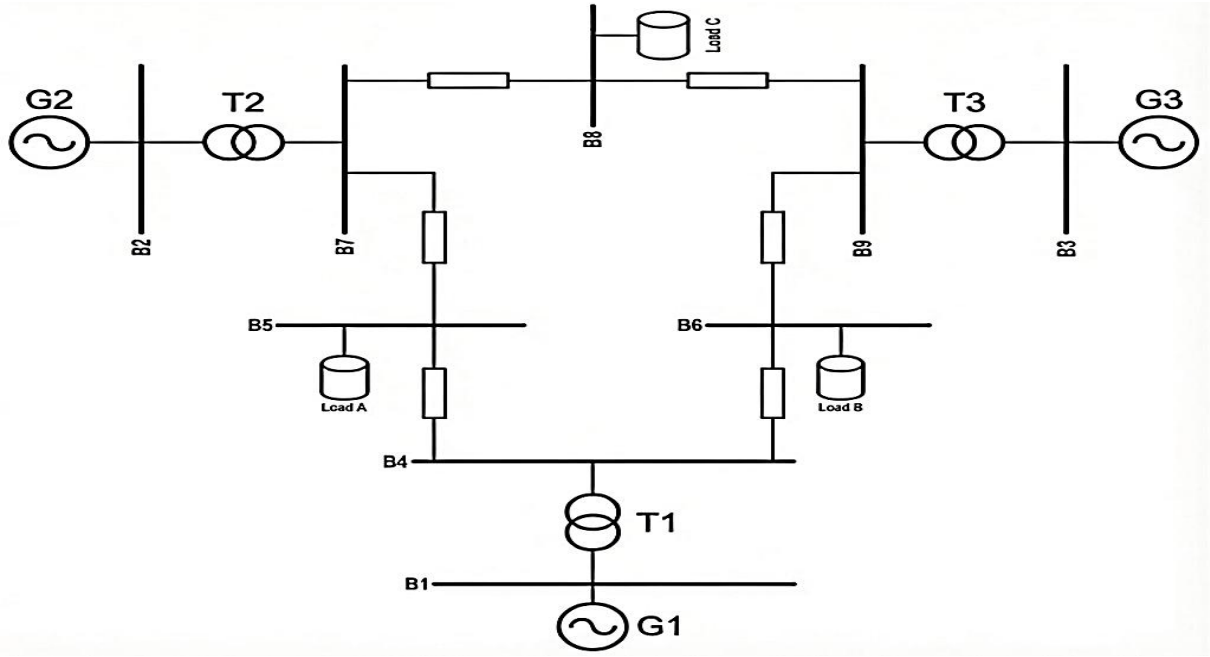

Figure 2: 9-bus test system

Table 1: Generator data of 9-bus test system

	Nominal Apparent Power[MVA]	Active power [MW]	Reactive Power [MVAr]	Load controller	Power Factor
Gen 1	247.5	71.6	27	Reference	0.85
Gen 2	192	163	6.7	Constant V	0.85
Gen 3	128	85	-10.9	Constant V	0.85

Table 2: Transformer data of 9-bus test system

Transformer	Rated Power (MVA)	Short Ckt Voltage uk(%)
T1	250	14.4
T2	200	12.5
T3	150	8.79

Table 3: Load data of 9-bus test system

Load	MW	MVAr
Load A	125	50
Load B	90	30
Load C	100	35

2.3 Integration of PV Sources

PV sources are integrated using the standard inverter-based PV model available in DIgSILENT PowerFactory. All PV units are operated in grid-following mode with active power control implemented through PQ control. In this study, three distributed PV units are connected at the load buses. PV penetration levels of 20%, 40%, and 60% are considered to represent lightly stressed, moderately stressed, and extremely low-inertia operating conditions, respectively. Equal distribution of PV generation among the load buses ensures a balanced representation of spatially distributed inverter-based resources. For each penetration level, the total PV contribution is adjusted accordingly, while the active power output of the synchronous generators is proportionally reduced to maintain system power balance.

Photovoltaic system does not consist of any rotating parts unlike conventional generator, with no rotating parts present, the PV system does not possess inherent inertia which is necessary to maintain the grid frequency stability during disturbances. Furthermore, Solar power is intermittent and most often non-dispatchable, as the Sun does not shine for all hours of the day in each location. As a result, high PV penetration reduces overall system inertia, leading to higher RoCoF and deeper frequency nadirs under contingencies. The PV penetration scenarios considered in this study are summarized in Table 4.

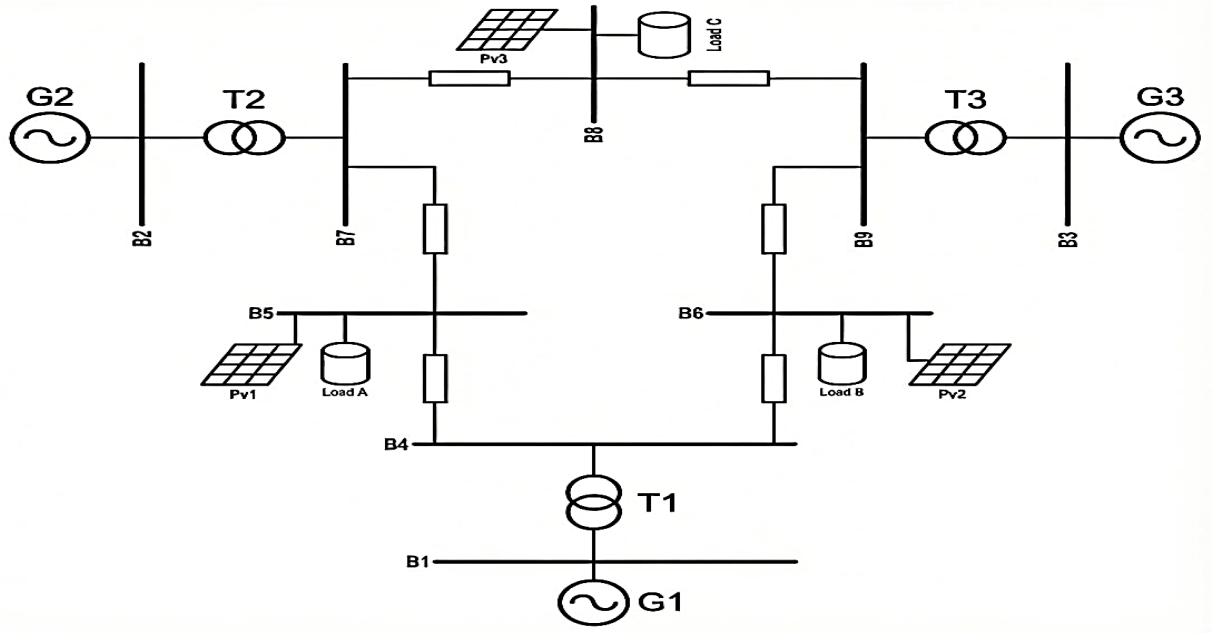

Figure 3: 9-bus test system with PV

Table 4: Distributed PV sources data

PV Penetration Level	PV on Load bus A (MW)	PV on Load bus B (MW)	PV on Load bus C (MW)	Total PV Power (MW)
20%	21.3	21.3	21.3	63.92

40%	42.61	42.61	42.61	127.84
60%	63.92	63.92	63.92	191.76

2.4 Contingencies

Contingencies are modelled as disturbances that cause sudden imbalances between generation and load, leading to frequency deviations. To evaluate the system's frequency response under realistic operating conditions, the following contingencies are considered.

Sudden Generator Outage: A generator outage represents the sudden disconnection of a synchronous generator, resulting in an instantaneous loss of generation. This creates a power imbalance that causes a rapid decline in system frequency.

Load variation in the grid: Load variation is introduced to analyze the impact of demand fluctuations on system frequency. In this study, the load of the selected buses is increased and decreased by ±10%.

2.5 Energy Storage Systems

Energy Storage System (ESS) have been widely proposed to compensate for the reduction in system inertia and damping caused by the displacement of conventional synchronous generators as they can emulate the dynamic behaviour of synchronous machines and provide fast acting support through function such as Inertial Response (IR) and Primary Frequency Reserve (PFR). ESS also helps reduce peak power demand by storing energy during low-demand periods and supplying it during peak hours thereby improving overall system efficiency and reliability (Amin *et al.*, 2021).

ESS that are potentially fast responding and have superior characteristics include super-capacitor, flywheels, Super Magnetic Energy Storage (SMES), CAES, BESS, and Pumped hydro energy storage. Battery Energy Storage System (BESS) are widely recognized as an effective technology for supporting frequency stability and are increasingly deployed in modern power systems (Amin *et al.*, 2021). The ESS is expressed as

$$P_{ESS} = S_{ESS}\,(P_{IR} + P_{PFR}) \tag{1}$$

2.5.1 ESS for Inertial Response

ESS can provide IR by acting as a source of virtual or synthetic inertia, where active power is rapidly injected into or absorbed from the grid in proportion to the RoCoF. This control mimics the kinetic energy release of synchronous generator, which helps to reduce the initial frequency drop after a disturbance. This fast response is especially important in low-inertia power systems with high renewable energy penetration, where conventional generator inertia is not sufficient to control RoCoF (Knap *et al.*, 2016). The inertial response of ESS is commonly expressed as

$$P_{IR} = K_{IR}\frac{df}{dt} \tag{2}$$

Where, P_{IR} represents the active power injected or absorbed by the ESS, K_{IR} is the inertial response gain that determines the magnitude of the power response, and $\frac{df}{dt}$ denotes the measured RoCoF.

The swing equation can be reformulated to define inertia constant (H_{ESS}) as follows (Knap *et al.*, 2016):

$$H_{ESS} = \frac{P_{IR} f_o}{2} . \left(\frac{df}{dt}\right)^{-1} \quad (3)$$

From the above two equations, the inertial constant H_{ESS} can be determined as,

$$H_{ESS} = \begin{cases} \frac{f_0}{2} . K_{IR,} & \text{if } |P_{IR}| \leq 1 \\ \frac{f_o}{2} . \left(\frac{df}{dt}\right)^{-1} & \text{if } |P_{IR}| \geq 1 \end{cases} \quad (4)$$

a) Sizing of IR:

The sizing of ESS for IR is determined by ensuring that the combined physical and synthetic inertia of the system is sufficient to limit RoCoF under a worst-case generation loss. This requirement can be represented by (Assery, Zhang and Chen, 2024).

$$\sum_{i=1}^{n} H_{ESSi} S_{ESSi} \geq \frac{\triangle P_{max} f_\circ}{2\frac{df_{max}}{dt}} - \sum_{i=1}^{n} H_i S_i \quad (5)$$

Where, $\triangle P_{max}$ is the maximum power imbalance, $f_\circ$ is the nominal frequency, and H_{sys} and S_{sys} denote the inertia and ratings of existing generators. This condition ensures that the ESS can effectively support frequency stability during the initial moments of disturbance.

2.5.2 ESS for Primary Frequency Response

PFR restores system frequency to a steady state level after the inertial response. ESS provide PFR by adjusting their active power output proportionally to the frequency deviation using a droop-based control, sharing the power imbalance with synchronous generators, and helping to prevent further frequency decline (Knap *et al.*, 2016). The primary frequency reserve of ESS is commonly expressed as

$$P_{PFR} \approx - \frac{f - f_\circ}{f_\circ R_{ESS}} \quad (6)$$

Where, f is the measured frequency, $f_\circ$ is the nominal frequency, and R_{ESS} is the droop setting.

a) Sizing of PFR:

The sizing of ESS for PFR ensures adequate power and energy to keep frequency within limits during disturbances. For a maximum power imbalance ΔP_{max}, the target power–frequency characteristic $\lambda_{target}$is defined as (Assery, Zhang and Chen, 2024):

$$\lambda_{target} = -\frac{\Delta P_{max}}{f_0 - f_{min}} \quad (7)$$

The actual system power–frequency characteristic under the largest contingency, λ_{CO}, is obtained from the combined droop response of the synchronous generators:

$$\lambda_{CO} = \sum_{1}^{N} \frac{1}{R_i S_i f_o} \quad (8)$$

To meet the required frequency performance, the ESS must provide the additional power–frequency characteristic $(\lambda_{target} - \lambda_{CO})$. Therefore, the ESS contribution for PFR can be expressed as:

$$\sum_{i=1}^{m} \frac{1}{R_{ESS,i} S_{ESS,i} f_0} \geq \lambda_{target} - \lambda_{CO} \quad (9)$$

Where, m is the number of ESS units and N is the number of synchronous generators. $R_{ESS,i}$ and $S_{ESS,i}$ are the droop coefficient and rated power of the i^{th} ESS unit, respectively, and f_0 is the nominal system frequency.

For a single ESS unit with droop coefficient R_{ESS}, the required ESS size for PFR reduces to:

$$S_{ESS} = (R_{ESS} f_0)(\lambda_{target} - \lambda_{CO}) \quad (10)$$

2.6 Battery Energy Storage System Modelling

Battery Energy Storage Systems introduced in the grid model at strategic buses provides frequency support under low-inertia conditions after PV generation (Sun *et al.*, 2024). The BESS is modelled in DIgSILENT PowerFactory using the standard BESS control template.

The model includes AC voltage, frequency, and PQ measurement blocks, which provides real-time system information to the control system. Frequency control generates a power reference based on grid frequency deviations, while the PQ controller determines the corresponding current reference. A battery model supplies voltage, current, and SoC information to the charge control unit, which ensures safe charging and discharging within operational limits. The converter block executes the current reference to enable controlled bidirectional power

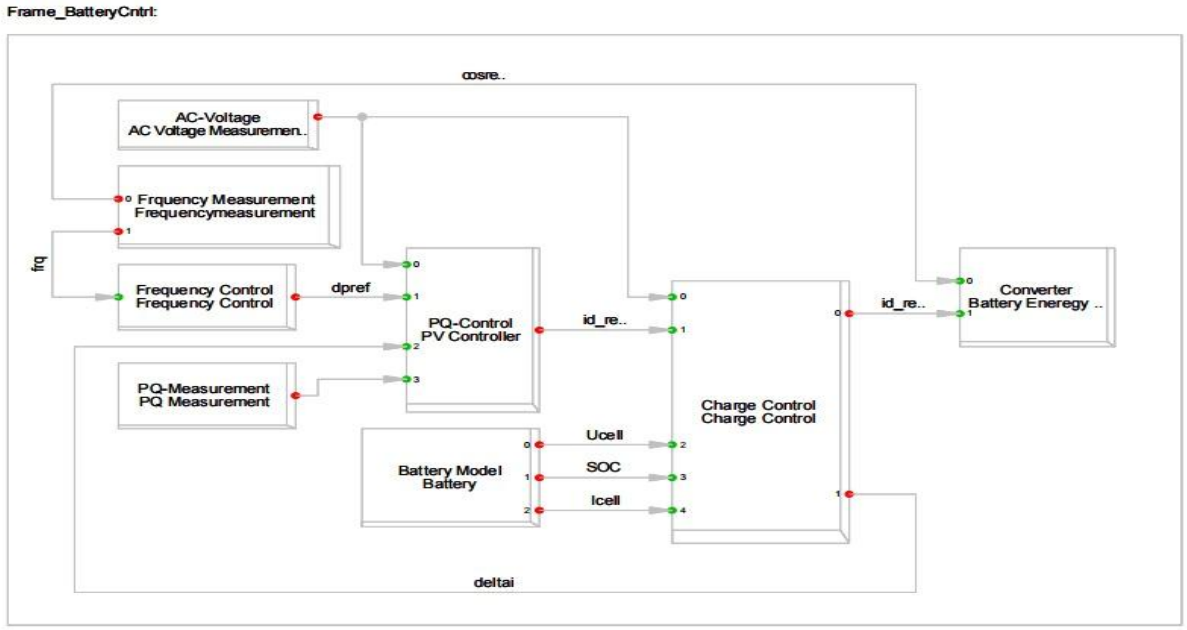

Figure 4: BESS Controller Frame available in DIgSILENT Power Factory

exchange between the battery and the grid. This coordinated control structure enables rapid active power injection or absorption to stabilize system frequency during disturbances. The BESS controller framework available in the DIgSILENT PowerFactory is shown in Figure 4.

2.6.1 Location of BESS

The effectiveness of BESS in providing synthetic inertia and frequency support strongly depends on its placement within the network. In this study, the BESS location is determined using a sensitivity analysis approach. Time-domain simulations are conducted under different PV penetration levels and contingency scenarios. Key performance indicators, including voltage magnitude, Rate of Change of Frequency, and frequency deviations are monitored to all buses. Buses exhibiting larger deviations during disturbances are identified as highly sensitive locations.

The bus with the lowest voltage magnitude and highest frequency sensitivity is selected as the most suitable location for BESS installation. Placing the BESS at this enhances voltage support and improves frequency stability through rapid active power injection or absorption.

2.6.2 Sizing of BESS

For a power system, the BESS is sized to ensure that frequency deviation, RoCoF, frequency nadir and steady-state frequency within acceptable operational limits under the largest contingency event.

For the IEEE 9-bus test system with 60% PV, the largest contingency is the loss of 10% of the total connected generation, corresponding to a generator outage of 31.96 MVA. This event is treated as the worst-case scenario for BESS sizing. Based on this disturbance magnitude and the system frequency response requirements, the BESS is sized to provide adequate IR and PFR. Knowing the system inertia, allowable RoCoF, frequency deviation limits and disturbance magnitude, the required BESS capacity for inertial response and primary frequency response is calculated.

3. Results and Discussion

The IEEE 9-bus system was modelled and integrated with PV generation to study its impact on system dynamics. Simulations are conducted in DIgSILENT PowerFactory version 15.1 on different computing platforms, including a Lenovo Ideapad and a Dell Insprion 16, to ensure computational consistency and validate results across hardware configuration.

3.1 Frequency Response of the 9-Bus Test System

The base system, consisting of all synchronous generators, was first simulated to establish the baseline frequency response. As shown in Figure 5, the system frequency dropped to a minimum value of 49.976 Hz at t = 3.460s and subsequently stabilized near 49.996 Hz. The high inertia contribution by the synchronous generators ensured a low RoCoF, keeping the overall frequency deviation within the acceptable operating limits.

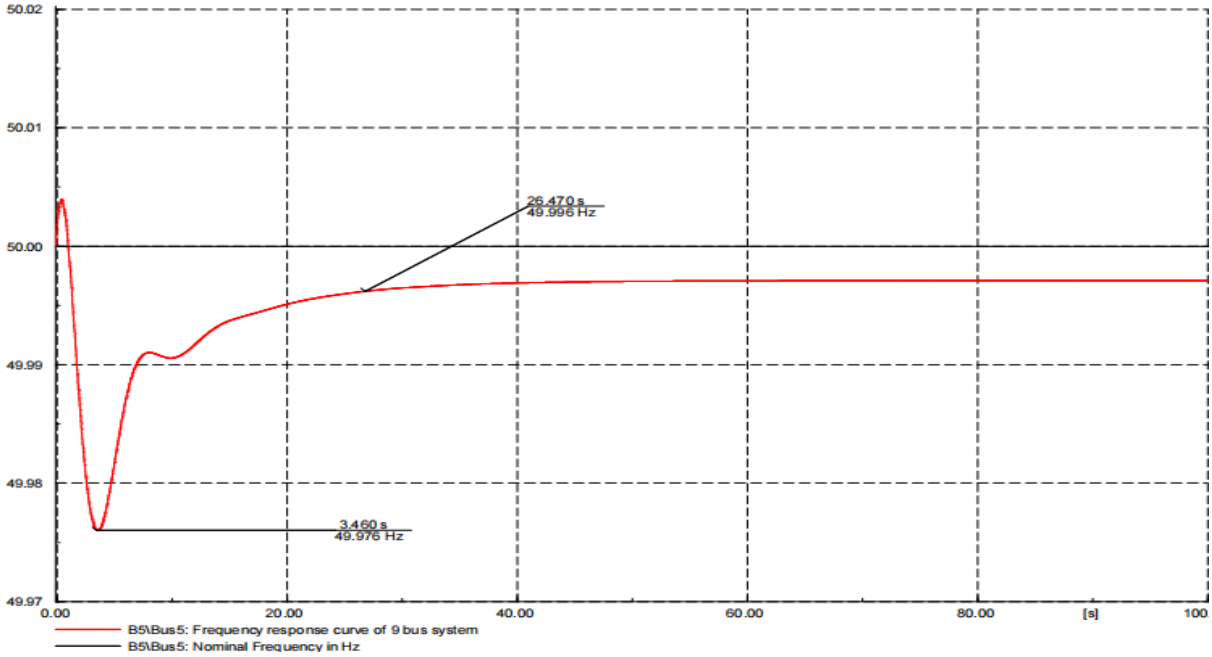

Figure 5: Frequency response curve of 9-bus test system

3.2 Frequency Response of the 9-Bus Test System with Varying PV Penetration

The system was simulated under PV penetration levels of 20%, 40%, and 60% to evaluate the impact of reduced inertia on frequency stability. As illustrated in Figure 6, the frequency response progressively deteriorated as PV penetration increases.

At 20% PV penetration, the frequency nadir decreased to 44.906 Hz, indicating a moderate loss of inertia. At 40% PV penetration, the nadir further declines to 42.962 Hz, while at 60% PV penetration, the frequency drops sharply to 40.434 Hz, accompanied by a significantly

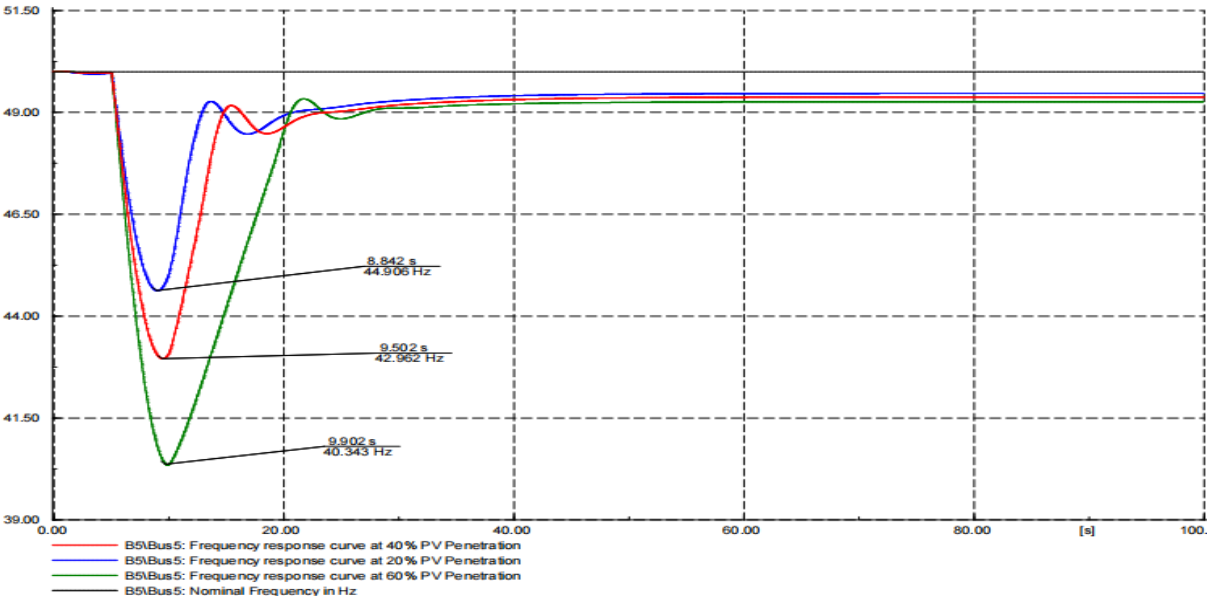

Figure 6: Frequency response curve with varying PV penetration

higher RoCoF. These results clearly demonstrated that high PV penetration severely weakens system frequency stability due to reduced inertial support. The increasing severity of frequency deviation highlights the growing vulnerability of low-inertia grids to disturbances.

Table 5: Frequency response of 9-bus test system with varying PV penetration

PV penetration	20%	40%	60%
Frequency nadir	44.906 Hz	42.962 Hz	40.343 Hz

3.3 Determination of the location of the BESS

The location of the Battery Energy Storage System was determined by evaluating the system operating conditions under high PV penetration and contingency events. Since the primary objective of the BESS in this study is to improve frequency stability through active power support, the system voltage profile was first examined to assess the need for reactive power support and to identify any weak buses.

Load flow analysis was performed for the low-inertia system with varying PV penetration levels using the Newton-Raphson method. The bus voltage magnitudes obtained under different contingency conditions at 60% PV penetration are summarized in Table 6.

Table 6: Bus voltage under different contingency cases at 60% PV penetration

Bus voltage in pu under different contingency cases at 60% PV penetration level			
Bus	**-10%**	**+10%**	**10% outage**
Bus 1	1.04	1.04	1.04
Bus 2	1.025	1.025	1.025
Bus 3	1.025	1.025	1.025
Bus 4	1.036	1.034	1.010
Bus 5	1.013	1.011	0.959
Bus 6	1.028	1.026	0.994
Bus 7	1.030	1.030	1.022
Bus 8	1.023	1.022	1.013
Bus 9	1.037	1.036	1.021

According to the grid code, a $\pm 5\%$ variation in the bus voltage is acceptable so, a bus with voltage level less than 0.95 pu is called a weak bus (Krishan and Suhag, 2019). From the load flow results, all bus voltages remained within the permissible range for all contingency cases. Therefore, reactive power support from the BESS is not required and the BESS is operated solely in active power control mode to provide synthetic inertia and primary frequency response.

Among all buses, Bus 5 consistently exhibited the lowest voltage magnitude, particularly under the outage condition, where the voltage drops to 0.959 pu. Bus 5 is also a load bus carrying the largest demand 125 MW and 50 MVAr in the system. Due to this high concentration, Bus 5 experiences the most significant impact during generation-load imbalance and contingency events. Placing the BESS at this bus allowed active power support to be delivered directly at the point of maximum load, which is highly effective for mitigating frequency deviations during disturbances. During sudden loss of generation or rapid PV output variation, the BESS can inject power at Bus 5, thereby reducing the effective power deficit seen by the system and improving the frequency nadir and RoCoF.

Considering its high load concentration, relatively low voltage under contingencies and suitability for high-voltage interconnection, Bus 5 at 230 kV is identified as the suitable location for integrating a large-scale BESS. Connecting the BESS at this bus ensures rapid and effective active power injection or absorption during power imbalance events, thereby significantly enhancing the system frequency response. Based on these considerations, Bus 5 was selected as the suitable location for BESS integration into the IEEE 9-bus test system.

3.4 Calculation and Integration of Optimal BESS Sizes

For the power system under study, the BESS was sized such that it limits key frequency response parameters, RoCoF, frequency nadir, and steady-state frequency deviation, within prescribed limits following the largest contingency event. In this project, a 10% generator outage at 60% PV penetration, corresponding to a power loss of 31.96 MW, was considered as the largest disturbance for calculating the BESS size.

According to ENTSO-E guidelines, the allowable RoCoF limit is less than 0.5 Hz/s, i.e. RoCoF<0.5 Hz and the steady-state frequency deviation should be limited to $\pm$0.2 Hz, i.e. $\Delta f_{ss} \leq 0.2$ Hz (Abuagreb, Abuhussein and Alzahir, 2021). The nominal frequency of the system is 50 Hz. The droop constant of the BESS is selected as 0.004. These limits formed the basis for determining the BESS size required to provide inertial response and primary frequency response.

Using these parameters, the BESS size required to provide IR and PFR is calculated. The BESS size was calculated considering the worst-case operating condition, as the maximum RoCoF and the lowest nadir occur at high PV penetration levels. In this study, the highest PV penetration corresponds to 191.96 MW, and the BESS size is calculated for this condition.

BESS Sizing for Inertial Response

Initial Response is required to limit the rate of change of frequency immediately after a disturbance, before primary frequency control becomes effective. The minimum inertia required to restrict RoCoF within acceptable limits was determined using the inertia balance condition given by the inertial response sizing criterion in equation 5.

For the IEEE 9-bus test system, the total inertia contributed from the synchronous generator is calculated as 2957. At higher PV penetration levels, only 40% of the synchronous generator inertia remains available, resulting in an effective system inertia is 1182.8. The remaining inertia requirements must therefore be supplied by the BESS. Using the BESS inertia constant obtained from inertial response model in equation 3-4, the minimum BESS rating required to satisfy the RoCoF constraint is calculated Based on the worst-case disturbance and the allowable RoCoF limit, the required BESS rating required for inertial response is found to be 33.89 MVA.

BESS Sizing for Primary Frequency Response

Primary Frequency Response is responsible for arresting the steady-state frequency deviation following a disturbance by adjusting active power output in proportion to frequency deviation. In this study, the BESS provides PFR through a droop-based control mechanism as described in equation 6.

The sizing of the BESS for PFR was carried out using the target power-frequency characteristics defined in equation 7. Based on the maximum power imbalance of 31.96 MW and the allowable steady-state frequency deviation of 0.2 Hz, the required system power-frequency slope is determined.

The power-frequency characteristic contributed by the synchronous generators under the largest contingency is evaluated using equation 8. The additional power-frequency support required from the BESS is then obtained using the sizing condition in equation 9. For a single BESS unit with a droop coefficient of 0.004, the required BESS rating is calculated using equation 10. Accordingly, the minimum BESS power rating required to provide adequate PFR is 31.96 MVA.

Integration of BESS

The BESS size requirements for inertial response and primary frequency response are 33.89 MVA and 31.96 MVA, respectively. Since these services may partially overlap, the largest power requirement was selected to ensure adequate frequency support under all operating conditions.

To account for converter losses, line losses, and practical implementation considerations, a 35 MVA BESS is selected. The BESS is integrated into the IEEE 9-bus test system at the 230kV Bus-5 through an 18/230kV step-up transformer to enhance frequency stability. During periods of excess generation, the BESS absorbs power to limit frequency rise, while during generation deficit, it injects power to arrest frequency decline. This coordinated operation enhances the overall frequency stability of the power system. Additionally, the selected placement at Bus-5 increases the effectiveness of frequency support by providing strong electrical coupling to both generation and load centers.

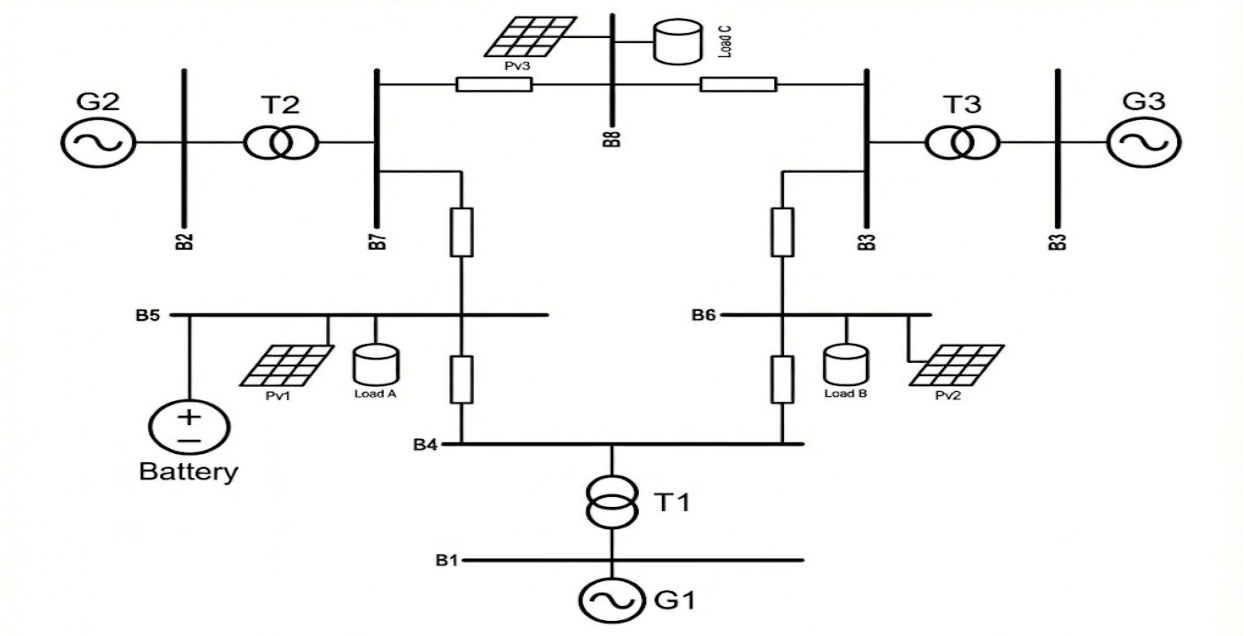

Figure 7: 9-bus test system with BESS

3.5 Varying level of PV Penetration

3.5.1 Frequency Response with 20% PV penetration

The frequency response of the system with 20% PV penetration was analyzed with and without integration of BESS, as shown in Figure 8. Without BESS, the frequency dropped to a nadir of 44.906 Hz at t = 9.212s, indicating a significant deviation from the nominal value. With BESS integration, the frequency nadir improved to 49.624 Hz, demonstrating a substantial reduction in frequency deviation. This improvement confirms that BESS effectively limits the frequency drop and enhances overall dynamic stability.

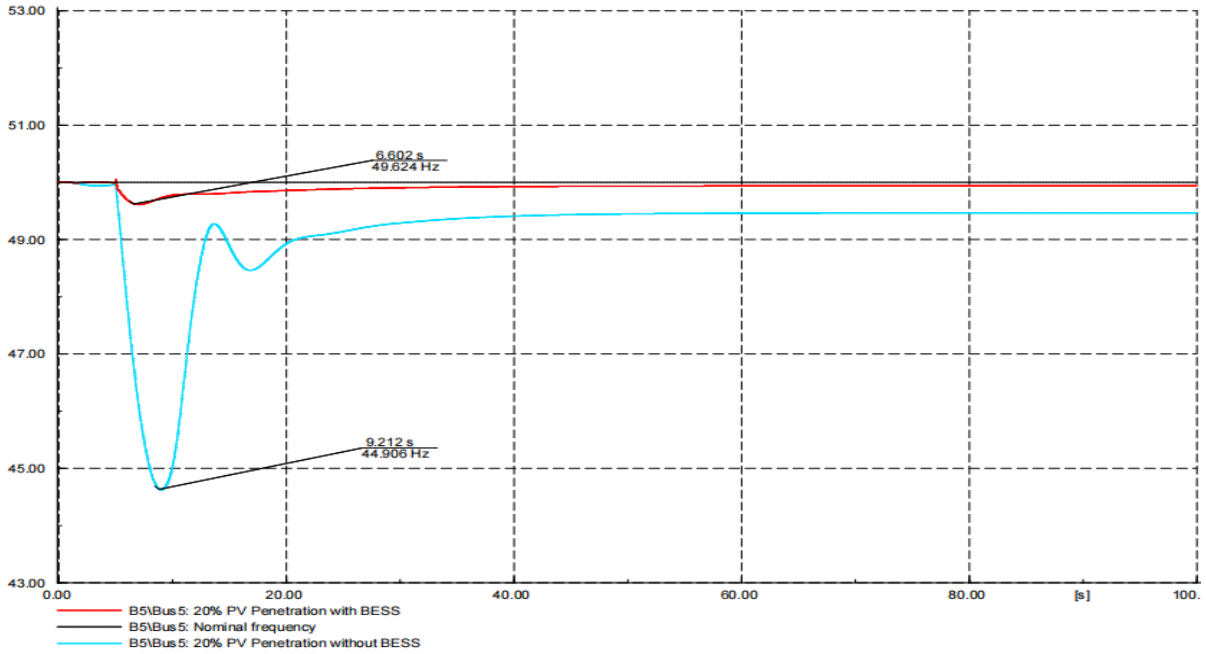

Figure 8: Frequency response curve with 20% PV penetration

Frequency Response of Generator Outage with 20% PV Penetration

Generator outage events of 10% and 20% were simulated to assess the effectiveness of BESS. For 10% generator outage, the frequency without BESS is dropped to 43.263 Hz at t = 9.152s, whereas with BESS the frequency nadir improved to 49.292 Hz at t =7.023s, with faster stabilization. Under 20% generator outage, the system without BESS experienced a critical frequency drop to 42.983 Hz at t =9.302s. With BESS, the frequency nadir increases to 48.981 Hz at t = 7.312s, keeping the system within acceptable operating limits.

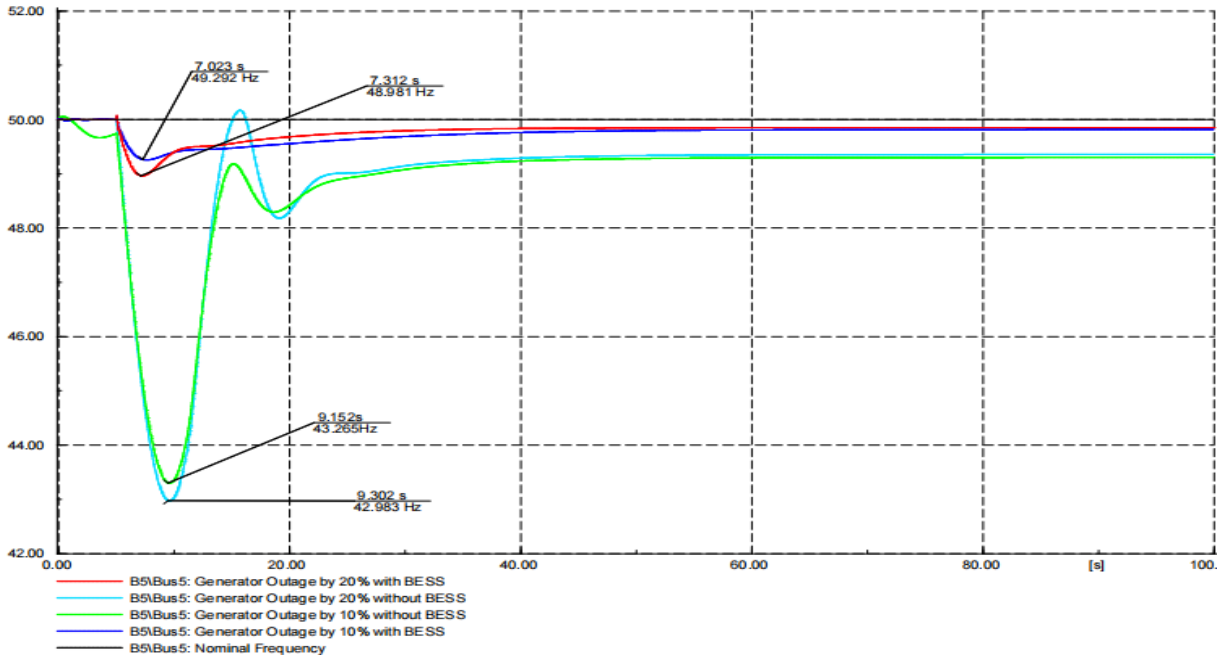

Figure 9: Frequency response curve of generator outage with 20% PV

Frequency Response of Load Variation with 20% PV Penetration

During a +10% load increase, the frequency nadir without BESS was 43.462 Hz at t = 9.112s, while BESS integration raised it to 49.301 Hz at t = 7.022s. Similarly, for -10% load variation, the frequency nadir improved from 45.611 at t = 8.382s to 49.892 Hz at t = 6.182s with BESS.

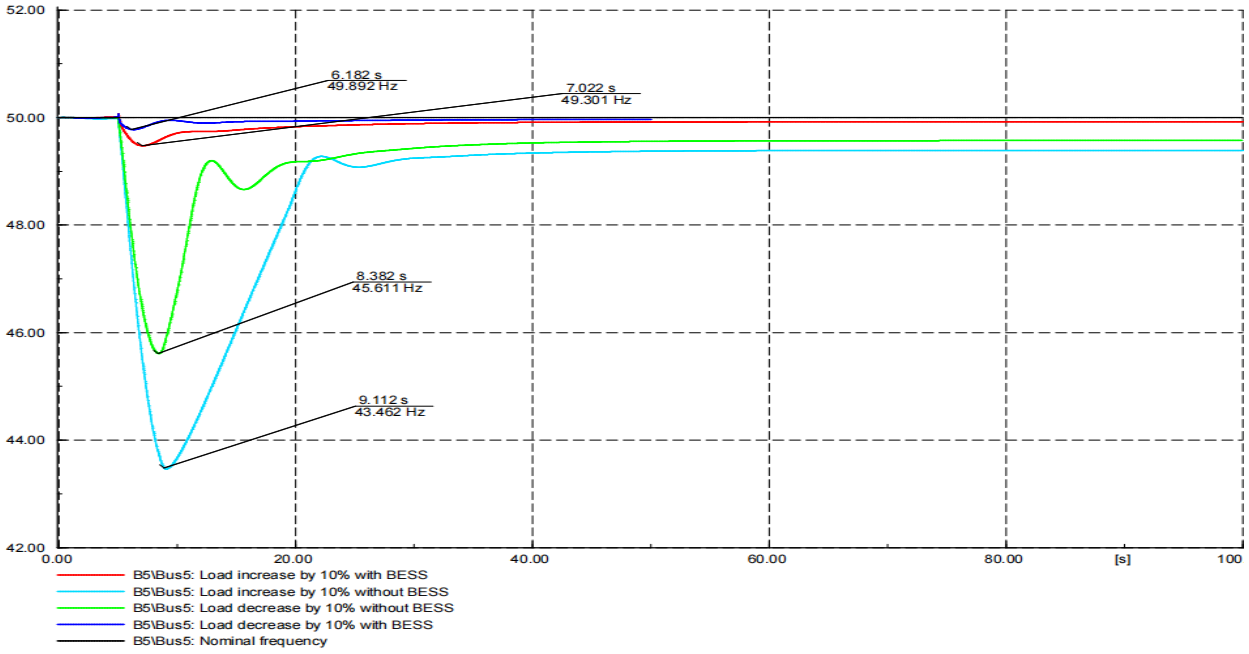

Figure 10: Frequency response curve of load variation with 20% PV

3.5.2 Frequency Response with 40% PV penetration

At 40% PV penetration, the system without BESS experienced a sharp frequency drop to 42.962 Hz at t = 9.372s, as shown in Figure 11. With BESS integration, the frequency nadir improved to 48.825 Hz at t = 7 .22s, demonstrating effective mitigation of low-inertia effects.

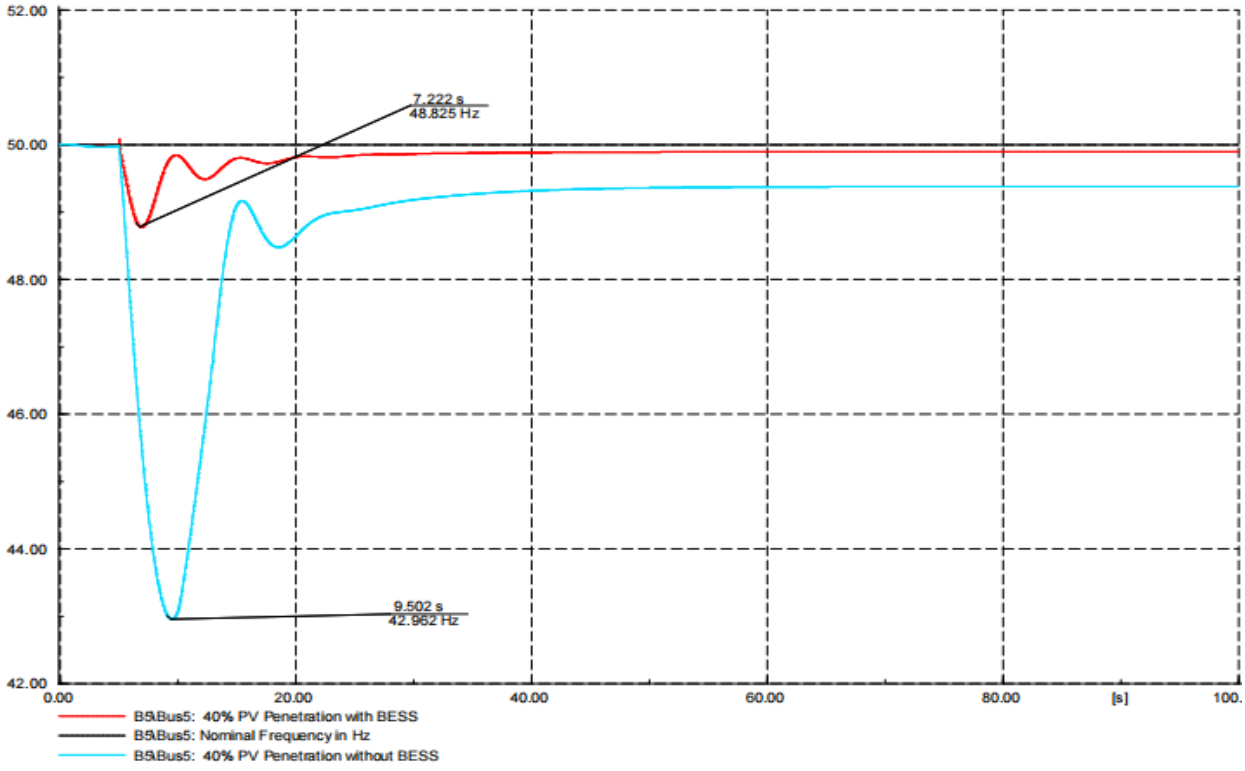

Figure 11: Frequency response curve with 40% PV penetration

Frequency Response of Generator Outage with 40% PV Penetration

For 10% generator outage, the frequency nadir without BESS was 40.677 Hz at t = 9.922s while with BESS it improved to 48.497 Hz at t = 7.472s. Under 20% generator outage, the frequency without BESS fell critically to 39.979 Hz at t = 10.472 s, whereas BESS raised the nadir to 48.361 Hz at t = 7.032 s, stabilizing the system within permissible limits.

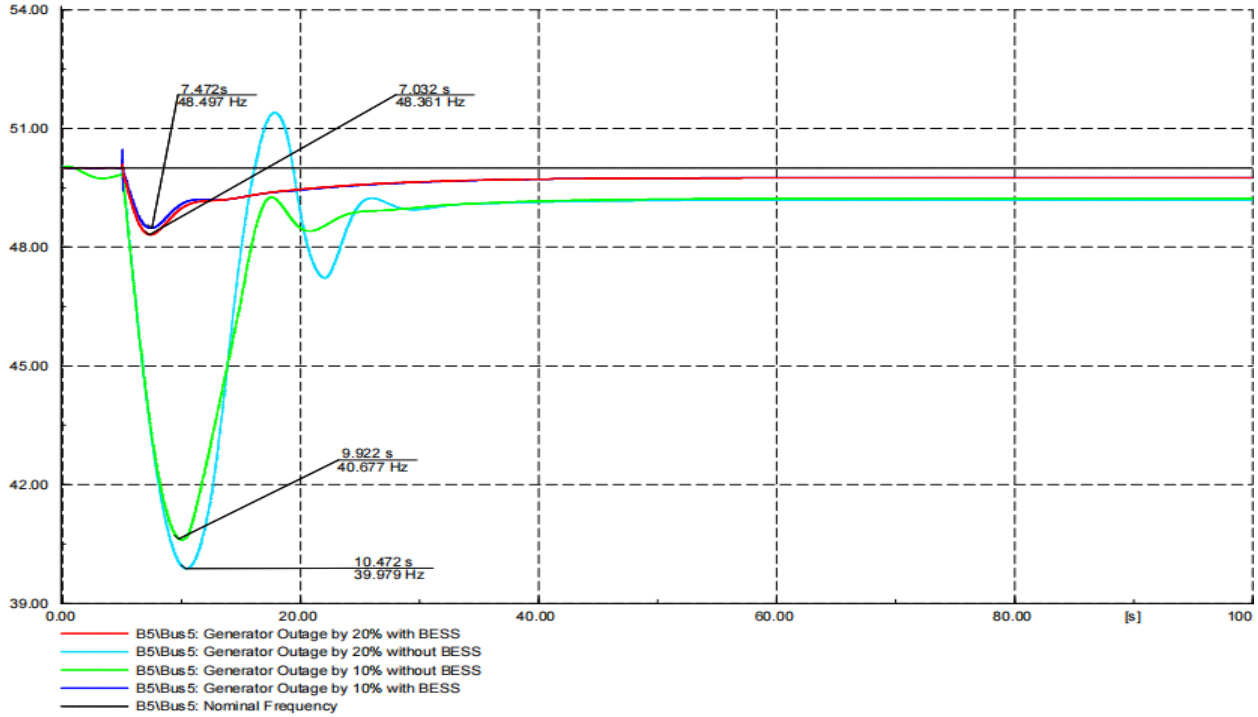

Figure 12: Frequency response curve of generator outage with 40% PV

Frequency Response of Load Variation with 40% PV Penetration

With +10% load increase, the frequency nadir improved from 41.997 Hz at t = 9.612s to 48.642 Hz at t = 6.682s with BESS. Similarly, during -10% load decrease, the frequency nadir increased from 44.669 Hz at t = 8.322s to 49.391 Hz at t = 6.872s, indicating enhanced damping and faster frequency recovery.

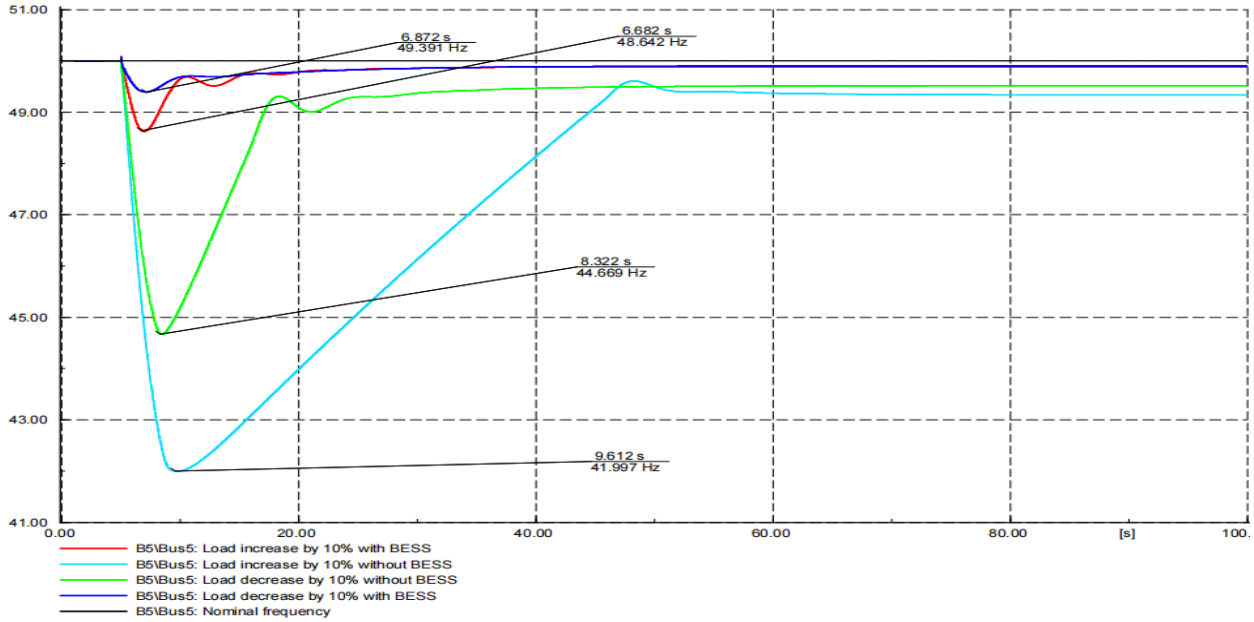

Figure 13: Frequency response curve of load variation with 40% PV

3.5.3 Frequency Response with 60% PV penetration

The system frequency response with 60% PV penetration represents extremely low-inertia conditions as illustrated in Figure 14. Without BESS, the frequency dropped sharply to 40.343 Hz at t = 9.892s, indicating severe instability. With BESS, the frequency nadir improved to 48.384 Hz at t = 7.222s, significantly enhancing system stability.

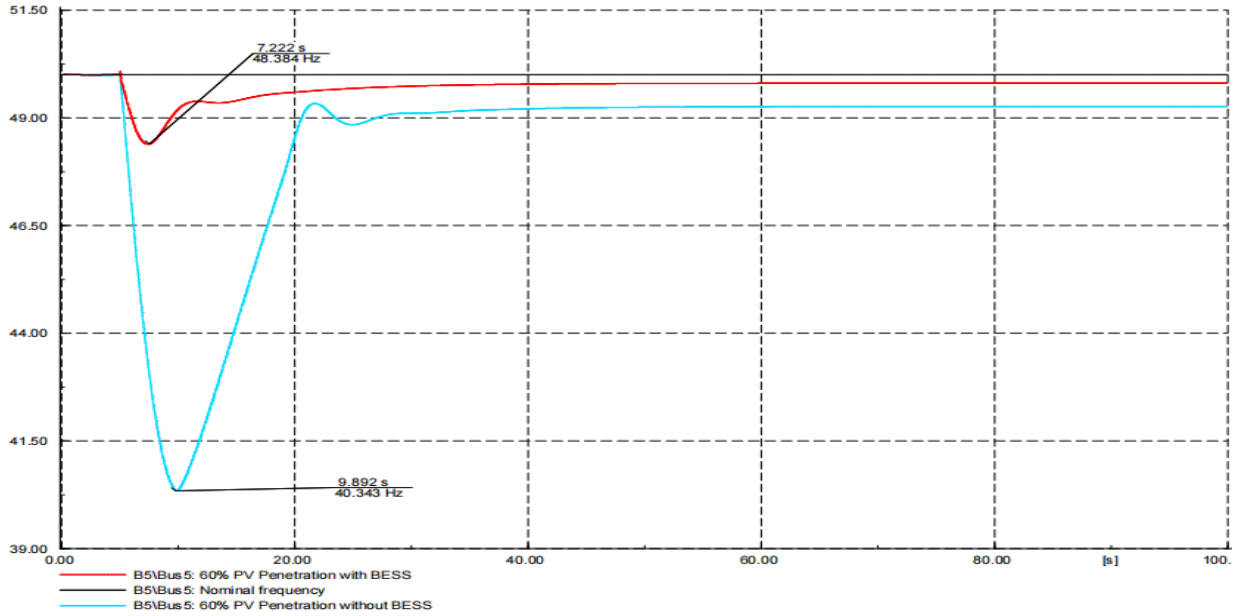

Figure 14: Frequency response curve with 60% PV penetration

Frequency Response of Generator Outage with 60% PV Penetration

For 10% generator outage, the system without BESS experienced a severe frequency drop to 39.770 Hz at t = 10.062s. With BESS, the frequency nadir improved to 48.207 Hz at t = 7.062s, demonstrating effective frequency support. A 20% generator outage led to excessive system instability, with the frequency falling below acceptable operational limits and therefore was excluded from further analysis.

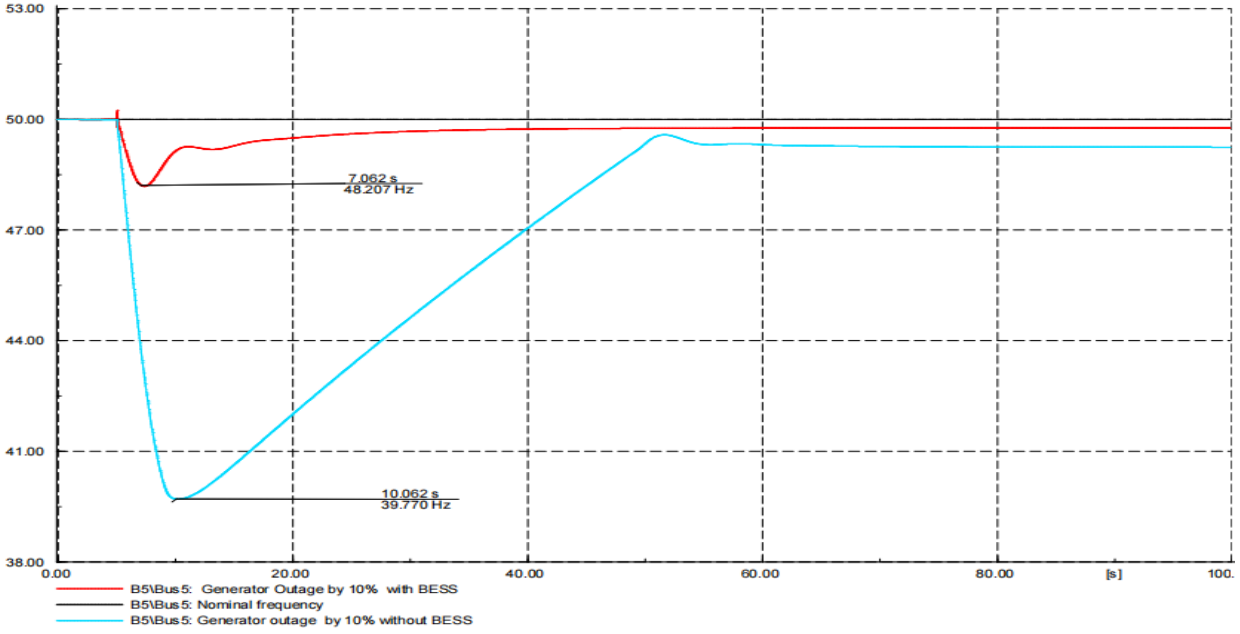

Figure 15: Frequency response curve of generator outage with 60% PV

Frequency Response of Load Variation with 60% PV Penetration

During +10% load increase, the frequency nadir improved from 39.936 Hz at t =1 0.882s to 48.291 Hz at t = 6.772s with BESS. Similarly, for -10% load decrease, the frequency nadir increased from 42.867 Hz at t = 8.442s to 48.780 Hz at t = 6.772s, accompanied by improved damping and faster recovery.

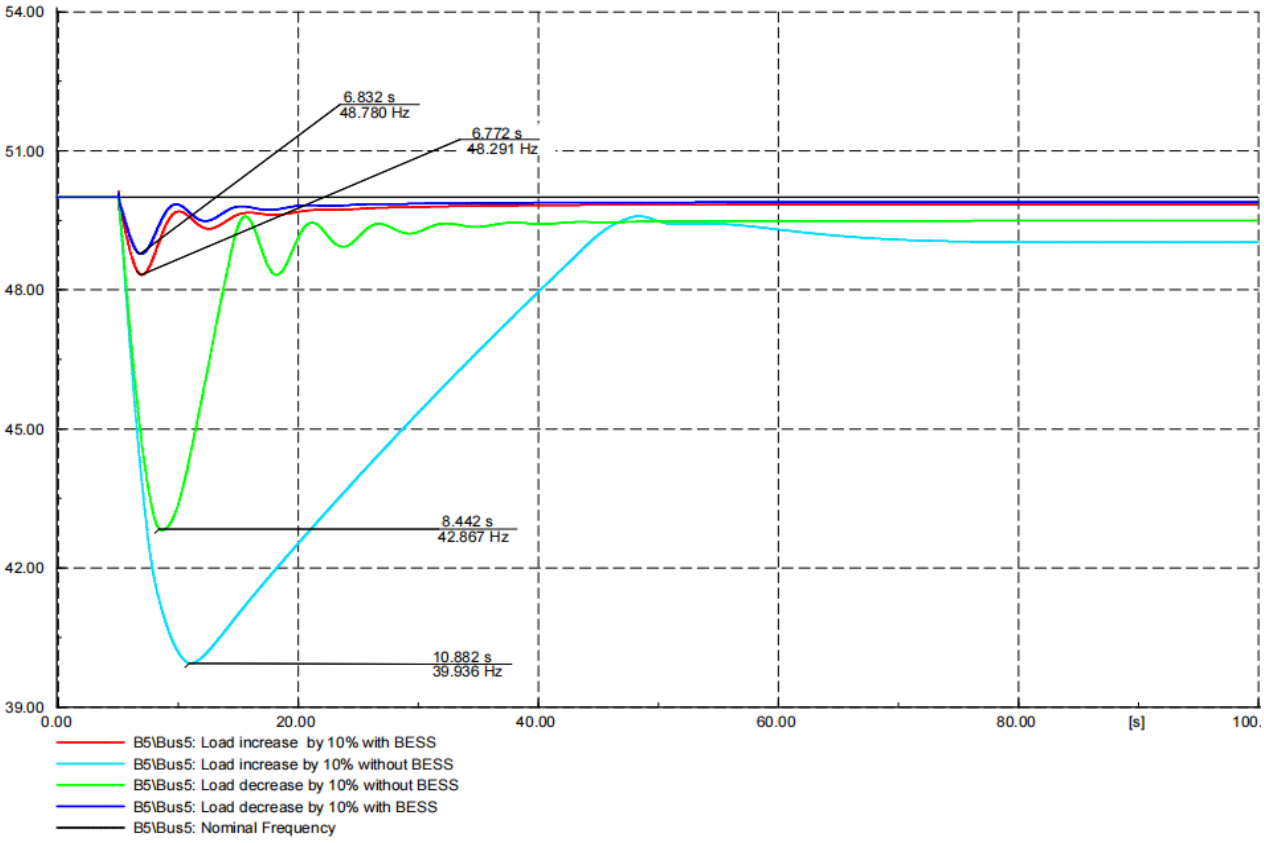

Figure 16: Frequency response curve of -10% load variation with 60% PV

3.6 Summary Table of Frequency Nadir of All Conditions

Table 7: Frequency nadir of all conditions

Scenario		Without BESS	With BESS
Varying 20% of PV Penetration		44.906 Hz	49.624 Hz
Contingency Event	Generator Outage (10%)	43.265 Hz	49.292 Hz
	Generator Outage (20%)	42.983 Hz	48.981 Hz
	Load Increases (+10%)	43.462 Hz	49.301 Hz
	Load Decreases (-10%)	45.611 Hz	49.892 Hz
Varying 40% of PV Penetration		42.962 Hz	48.825 Hz
Contingency Event	Generator Outage (10%)	40.677 Hz	48.497 Hz
	Generator Outage (20%)	39.979 Hz	48.361 Hz
	Load Increases (+10%)	41.997 Hz	48.642 Hz
	Load Decreases (-10%)	44.669 Hz	49.391 Hz
Varying 60% of PV Penetration		40.343 Hz	48.384 Hz
Contingency Event	Generator Outage (10%)	39.770 Hz	48.207 Hz
	Load Increases (+10%)	39.936 Hz	48.291 Hz
	Load Decreases (-10%)	42.867 Hz	48.780 Hz

4 Conclusion

The global energy sector is undergoing a rapid transition as climate goals and environmental concerns drive the large-scale integration of renewable energy sources, particularly solar PV generation. While this transition supports sustainability objectives, it also introduces significant challenges to power system frequency stability due to the reduction of system inertia resulting from the displacement of synchronous generators.

This project analyzed the impact of high PV penetration on frequency stability using a modified IEEE 9-bus test system modelled in DIgSILENT PowerFactory. Time-domain simulations were conducted for PV penetration levels of 20%, 40%, and 60%, considering various contingency scenarios such as generator outages and load variations. The results demonstrated that increasing PV penetration reduces system inertia, leading to higher RoCoF, deeper frequency nadirs, and slower post-disturbance recovery. At higher penetration levels, frequency deviations became critically unstable, highlighting that PV generation alone is insufficient to maintain frequency stability during sudden disturbances.

To address these low-inertia challenges, a 35 MVA BESS was implemented for the IEEE 9-bus system. Using the swing equation and related analytical formulas, the BESS size was determined to ensure adequate frequency support. After BESS implementation, the frequency response parameters including RoCoF, frequency nadir and steady-state frequency deviation improved significantly, remaining within Nepal's operational limits of ±5% of the nominal frequency under all scenarios (Electricity Regulatory Commission, 2024).

These results confirm that BESS with synthetic inertia emulation and droop-based frequency control provides a technically robust, flexible and fast-acting solution to enhance frequency stability in PV-dominated power systems. The study demonstrates that systematic assessment of PV penetration levels, contingencies analysis, and appropriate BESS sizing can effectively maintain frequency stability, accelerate post-disturbance recovery and improve dynamic system performance.

The methodology and findings of this study can be applied to the planning and operation of low-inertia power systems with high penetration of renewable generation. The proposed BESS

sizing and frequency control approach can assist system operators and planners in determining minimum storage requirements for fast frequency response, contingency management and grid code development. This framework is particularly relevant for power systems such as Nepal's grid, where large-scale solar integration is planned alongside conventional hydropower generation.

Future enhancements of this work may include extending the analysis to larger and more realistic network models, incorporating advanced control techniques such as adaptive droop control and grid-forming inverter operation, and evaluating coordinated frequency control between hydropower plants and BESS. Additional research could also focus on optimal BESS placement, economic feasibility, and real-time or hardware in the loop simulations to further assess system performance under practical operating conditions.

References

- Wiatros-Motyka, M., Fulghum, N., Jones, D., et al. (2024) Global Electricity Review 2024. London: Ember Energy.
- International Energy Agency (2025) Electricity – Global Energy Review 2025. Paris: International Energy Agency.
- Amin, M.R., Negnevitsky, M., Franklin, E., Alam, K.S. and Naderi, S.B. (2021) 'Application of battery energy storage system for primary frequency control in power systems with high renewable energy penetration', Energies, 14(5), Article 1379.
- Assery, S.A., Zhang, X.-P. and Chen, N. (2024) 'Large-scale BESS for damping frequency oscillations of power systems with high wind power penetration', Inventions, 9(1), Article 3.
- Chunyang, Z., Andersen, P.B., Træholt, C. and Hashemi, S. (2023) 'Grid-connected battery energy storage system: A review on application and integration', Renewable and Sustainable Energy Reviews, 182, Article 113400. doi:10.1016/j.rser.2023.113400.
- Anderson, P.M. and Fouad, A.A. (2003) Power System Control and Stability. 2nd edn. Piscataway, NJ: IEEE Press.
- Department of Hydropower and Indian Institute of Technology Roorkee (n.d.) 'Hydro generator characteristics and performance', in Modern Hydroelectric Engineering, Vol.
- IEEE Power System Dynamic Performance Committee (1992) 'Hydraulic turbine and turbine control models for system dynamic studies', IEEE Transactions on Power Systems, 7(1), pp. 167–179.
- Energy Education (n.d.) 'Solar power'. Available at: https://energyeducation.ca/encyclopedia/Solar_power (Accessed: 25 November 2025).
- Knap, V., Chaudhary, S.K., Stroe, D.-I., Swierczynski, M., Craciun, B.-I. and Teodorescu, R. (2016) 'Sizing of an energy storage system for grid inertial response and primary frequency reserve', IEEE Transactions on Power Systems, 31(5), pp. 3447–3456.

- Sun, Y., et al. (2024) 'The frequency regulation control method of large-scale distributed energy storage systems in the smart grid', Elektronika ir Elektrotechnika, 30(5), pp. 14–21. doi:10.5755/j02.eie.38186.
- Krishan, O. and Suhag, S. (2019) 'An updated review of energy storage systems: Classification and applications in distributed generation power systems incorporating renewable energy resources', International Journal of Energy Research, 43(12), pp. 6171–6210.
- Abuagreb, M., Abuhussein, A. and Alzahir, S. (2021) 'Sizing of energy storage systems for virtual inertia emulation', Energies, 14(13), Article 4002.
- Electricity Regulatory Commission (2024) Annual Report 2080/81. Kathmandu: Electricity Regulatory Commission. Available at: https://api.erc.gov.np/media/documents/ERC-Annual-Report-2080-81.pdf (Accessed: 22 February 2026).